Article
Beitr. Phys. Atmosph., February 1991, p. 13–25
0005-8173/91/01 0013–13 $ 3.00/0
Vol. 64, No. 1

Intercomparison of Two Models for the Dispersion of Chemically Reacting Pollutants

by J. GRAF[1] and N. MOUSSIOPOULOS[2]

[1] Meteorologisches Institut, Universität München, FRG
present address: Institut für Physik der Atmosphäre, DLR Oberpfaffenhofen, FRG

[2] Institut für Technische Thermodynamik, Universität Karlsruhe, FRG
present address: Laboratory of Heat Transfer, Department of Mechanical Engineering, Aristotle University Thessaloniki, Greece

(Manuscript received March 1989; in revised form February 1991)

Abstract

Comparative model simulations were performed to estimate the feasible error caused by operator splitting methods. For this purpose the one-dimensional diffusion equation system for chemically reacting pollutants was solved for a specified reference case with two different models. In one of these models the operator splitting method is used, in the other the equation system is solved without decoupling diffusion and chemistry. Although in a qualitative sense the results of the two models are in good agreement, application of the operator splitting method leads to an underprediction of the ozone concentration, especially at a low photochemical smog potential. This underestimation of the ozone level is supported by simple analytical considerations and is confirmed by additional numerical simulations.

Zusammenfassung

Vergleich zweier Modelle für die Ausbreitung chemisch aktiver Schadstoffe

Zur Klärung der Frage, inwieweit eine getrennte Behandlung der Operatoren die Ergebnisse numerischer Simulationen beeinflußt, wurden vergleichende Modellrechnungen durchgeführt. Hierzu wurde für einen Referenzfall das System eindimensionaler Diffusionsgleichungen für chemisch aktive Schadstoffe mit zwei unterschiedlichen Modellen gelöst – einmal mit einer Operatorentrennung, und zum anderen ohne Entkopplung von chemischer Reaktionskinetik und Vertikaltransport durch turbulente Diffusion. Obwohl die Ergebnisse der zwei Modelle qualitativ gut übereinstimmen, führt die Zerlegung der Operatoren zu einer Unterschätzung der Ozonkonzentration, besonders bei niedrigem Photosmog-Potential. Die Ergebnisse des Modellvergleichs werden durch vereinfachte analytische Überlegungen und zusätzliche numerische Simulationen bestätigt.

1 Introduction

For simulations of the dispersion of J chemically reacting pollutants a system of J nonlinear transport differential equations has to be solved. Following K-theory to describe turbulent diffusion, the system takes the form

$$\frac{\partial \mathbf{c}}{\partial t} + \nabla \cdot (\mathbf{v}\mathbf{c}) = \nabla \cdot (\mathbf{K}_c \nabla \mathbf{c}) + \mathbf{R} + \mathbf{S} \qquad (1)$$

where $\mathbf{c} \equiv (c_1, c_2, ..., c_j)^T$ is the vector of the pollutant concentrations, $\mathbf{v}$ the wind velocity vector, $\mathbf{K}_c$ the eddy diffusivity tensor, $\mathbf{R}$ the vector of chemical production (or destruction) terms and $\mathbf{S}$ the vector of other source (or sink) terms. Equation system (1) is usually solved for known meteorological variables (wind velocity, temperature, humidity, eddy diffusivity), i.e. the mass conservation equations are normally decoupled from the equation of motion of air. Hence, any dependence of the eddy diffusivity on the kinetics of the chemical reaction mechanism is neglected (cf. Lamb, 1973).

For a proper consideration of the underlying orography, equation system (1) is usually transformed to terrain following coordinates. The resulting equation is solved numerically for the specified initial and boundary conditions. One of the major difficulties associated with the numerical solution is the stiffness of the considered semi-discrete equation systems (McRae et al., 1982). Hence, implicit solution procedures are far superior for the time integration. However, this can lead to an enormous computational task in the case of multidimensional problems, as very large sparse matrices have to be inverted. Therefore, the multidimensional problem is usually reduced to a sequence of

simpler problems by employing operator splitting, i.e. by decomposing the original operator in a number of elemental components.

In spite of its undoubted advantages, operator splitting has the short-coming of causing an intrinsic error as, strictly speaking, the computed results do not represent anymore the solution of equation system (1). In principle, operator splitting should be always justified by estimating the magnitude of the intrinsic error. This, however, is a rather difficult task and is therefore usually omitted.

As an alternative in estimating the intrinsic error, characteristic times for elemental processes are frequently used to compare the speed of these processes and to prove the applicability of operator splitting. Thus, advective and horizontal diffusive transport can be shown to be rather slow compared to vertical diffusive transport and chemistry (Moussiopoulos, 1987). It seems, therefore, to be justifiable to split advection and horizontal diffusion from vertical diffusion and chemical kinetics. The latter, however, have comparable characteristic times and it is not a priori clear whether operator splitting is permissible or not.

In this paper we analyse in detail the consequences of splitting vertical diffusion and chemical kinetics. For this purpose we solve for a specified reference case the spatially one-dimensional diffusion equation system for chemically reacting pollutants

$$\frac{\partial \mathbf{c}}{\partial t} = \frac{\partial}{\partial z}\left(K_{zz}\frac{\partial \mathbf{c}}{\partial z}\right) + \mathbf{R} + \mathbf{S} \qquad (2)$$

using two different models,

- the one-dimensional model of Graf (1990) adopting operator splitting (henceforth: Munich model) and
- the spatially one-dimensional version of the dispersion model MARS (**M**odel for the **A**tmospheric Transport of **R**eacting **S**pecies; Moussiopoulos, 1987 and 1989) where operator splitting is avoided (henceforth: Karlsruhe model).

In the next section a brief description of both models is given. Subsequently, the considered reference case is outlined and simulation results are presented in detail. In the final section we summarize conclusions from the comparison of the results.

2 Description

2.1 Munich Model

Using the operator splitting procedure (McRae et al., 1982), the spatially one-dimensional diffusion equation (2) can be written in the form:

$$\frac{\partial \mathbf{c}}{\partial t} = \frac{\partial}{\partial z}\left(K_{zz}\frac{\partial \mathbf{c}}{\partial z}\right) + \mathbf{S} \qquad (3)$$

$$\frac{\partial \mathbf{c}}{\partial t} = \mathbf{R} \equiv \mathbf{f}(t, c_1, c_2, ..., c_J) \qquad (4)$$

If D and C are the numerical approximations of the diffusion and the chemical operators, the solution at the time t_{n+1} is:

$$\mathbf{c}(t_{n+1}) = C\,\mathbf{c}^*(t_{n+1}) \qquad (5)$$

$$\mathbf{c}^*(t_{n+1}) = D\,\mathbf{c}(t_n) \qquad (6)$$

Eq. (4) has to be integrated at every vertical grid point with initial values from the results of Eq. (3) which is solved with the ADE procedure (Roache, 1976). Chemistry is decoupled from diffusion and is solved for the period Δt, i.e. the time step for the integration of the diffusion step. For solving Eq. (4), the Gear algorithm is used without assuming pseudo-steady-state-approximations. The model assumes an equidistant grid with the concentrations defined at the cell centers

$$z_k = (k - 0.5)\,\Delta z; \qquad k = 1, 2, ..., K \qquad (7)$$

(Figure 1). To assure conservative properties fluxes are computet at the height levels

$$\zeta_k = k\,\Delta z; \qquad k = 1, 2, ..., K \qquad (8)$$

An additional grid point is introduced below the surface to incorporate ground level sources. At the upper boundary the mass transfer is neglected, i.e.

$$\left.\frac{\partial \mathbf{c}}{\partial z}\right|_T = 0 \qquad (9)$$

2.2 Karlsruhe Model

In the following, a brief summary of the Karlsruhe model is given. More detailed description may be found elsewhere (Moussiopoulos, 1987 and 1989).

The solution of equation system (2) with the Karlsruhe model is based on the assumption that the turbulent eddy diffusivity K_{zz} is identical for all considered species. Arbitrary non-equidistant grid spacings are possible in the vertical direction. With the notation as in Figure 1 one gets the second order difference approximation

$$g_j(t, c_{jk-1}, c_{jk}, c_{jk+1}) \equiv$$

$$\frac{1}{\Delta\zeta_k}\left[K_{zz}(t, \zeta_k)\frac{c_{jk+1} - c_{jk}}{\Delta z_k} - K_{zz}(t, \zeta_{k-1})\frac{c_{jk} - c_{jk-1}}{\Delta z_{k-1}}\right] \qquad (10)$$

for the diffusion term of the j-th species. It is of decisive importance for the algorithm included in the Karlsruhe

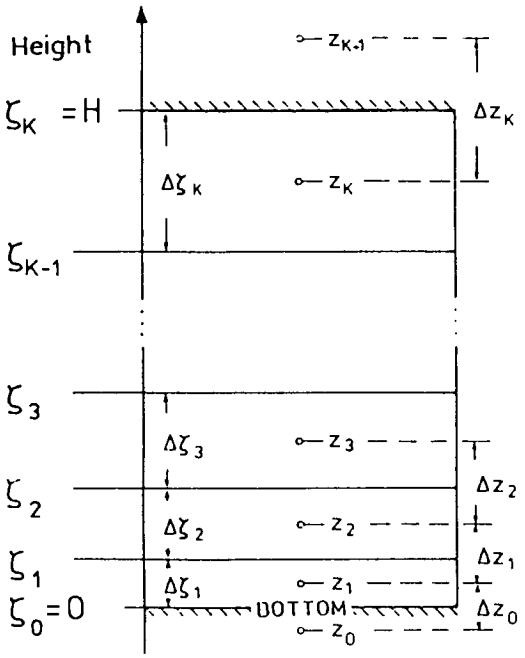

Figure 1 Vertical grid definition.

model that the discrete operator g_j is linear and that it depends only on the concentration of the j-th species at the cells k-1, k and k+1.

With the abbreviation f_j for the sum $R_j + S_j$, the semi-discrete formulation of (2) for the j-th species at the k-th grid cell takes the form

$$P_j(c_{jk-1}, \mathbf{c}_k, c_{jk+1}) \equiv$$

$$c'_{jk} - f_j(t, \mathbf{c}_k) - g_j(t, c_{jk-1}, c_{jk}, c_{jk+1}) = 0 \qquad (11)$$

with $\mathbf{c}_k \equiv (c_{1k}, c_{2k}, ..., c_{Jk})$ as the vector of the unknown concentrations at the k-th grid cell. Using vector notation one gets for all considered species at that cell

$$\mathbf{P}(\mathbf{c}, k) \equiv \mathbf{c}'_k - \mathbf{f}(t, \mathbf{c}_k) - \mathbf{g}(t, \mathbf{c}_{k-1}, \mathbf{c}_k, \mathbf{c}_{k+1}) = 0 \qquad (12)$$

with $\mathbf{c} \equiv (\mathbf{c}_1, \mathbf{c}_2, ..., \mathbf{c}_K)$. Together with appropriate initial and boundary conditions the equation system (12) corresponds to an initial/boundary value problem. This problem is solved with a selfadaptive predictor-corrector method: The derivatives $\mathbf{c}'_k$ are approximated by backward difference formulae, while predictor formulae are used to obtain first estimates for the unknowns at the next time level. These estimates are corrected in the course of a Newton iteration based on the nonlinear discrete operator (k = 1, 2, ..., K)

$$\mathbf{P}_D(\mathbf{y}_n, k) \equiv \mathbf{y}'_{k,n} - \mathbf{f}(t_n, \mathbf{y}_{k,n}) -$$

$$- \mathbf{g}(t_n, \mathbf{y}_{k-1,n}, \mathbf{y}_{k,n}, \mathbf{y}_{k+1,n}) = 0 \qquad (13)$$

where $\mathbf{y}_n \equiv (\mathbf{y}_{1,n}, \mathbf{y}_{2,n}, ..., \mathbf{y}_{K,n})^T$ is the discrete approximation for the exact solution $\mathbf{c}$ at the time level t_n. During the iteration it is required that

$$\mathbf{P}_D(\mathbf{y}_n^{\nu+1}, k) \equiv \mathbf{P}_D(\mathbf{y}_n^{\nu} + \Delta\mathbf{y}_n^{\nu+1}, k) \stackrel{!}{=} 0 \qquad (14)$$

A Taylor expansion yields after neglecting higher order terms

$$\mathbf{y}'^{\nu}_{k,n} + \Delta\mathbf{y}'^{\nu+1}_{k,n} - \mathbf{f}(t_n, \mathbf{y}^{\nu}_{k,n}) -$$

$$\underbrace{- \frac{\partial \mathbf{f}}{\partial \mathbf{y}_{k,n}}(t_n, \mathbf{y}^{\nu}_{k,n})}_{\mathbf{F}'^{\nu}_{k,n}} \Delta\mathbf{y}^{\nu+1}_{k,n} -$$

$$\underline{\underline{- \mathbf{g}(t_n, \mathbf{y}^{\nu}_{k-1,n}, \mathbf{y}^{\nu}_{k,n}, \mathbf{y}^{\nu}_{k+1,n})}} - \qquad (15)$$

$$\underbrace{- \frac{\partial \mathbf{g}}{\partial \mathbf{y}_{k-1,n}}(t_n)}_{\mathbf{G}'^{d}_{k,n}} \cdot \Delta\mathbf{y}^{\nu+1}_{k-1,n} \underbrace{- \frac{\partial \mathbf{g}}{\partial \mathbf{y}_{k,n}}(t_n)}_{\mathbf{G}'_{k,n}} \cdot \Delta\mathbf{y}^{\nu+1}_{k,n} -$$

$$\underbrace{- \frac{\partial \mathbf{g}}{\partial \mathbf{y}_{k+1,n}}(t_n)}_{\mathbf{G}'^{u}_{k,n}} \cdot \Delta\mathbf{y}^{\nu+1}_{k+1,n} = 0$$

$\mathbf{F}'^{\nu}_{k,n}$ is the numerical approximation of the Jacobian at the k-th grid cell. For the matrices $\mathbf{G}'^{d}_{k,n}$, $\mathbf{G}'_{k,n}$ und $\mathbf{G}'^{u}_{k,n}$ one gets, because of Eq. (10), multiples of the unit matrix, i.e.

$$\mathbf{G}'^{d}_{k,n} \equiv -d_k \cdot \mathbf{I}; \qquad d_k = -\frac{K_{zz}(t, \zeta_{k-1})}{\Delta\zeta_k \Delta z_{k-1}} \qquad (16a)$$

$$\mathbf{G}'^{u}_{k,n} \equiv -u_k \cdot \mathbf{I}; \qquad u_k = -\frac{K_{zz}(t, \zeta_k)}{\Delta\zeta_k \Delta z_k} \qquad (16b)$$

$$\mathbf{G}'_{k,n} \equiv -m_k \cdot \mathbf{I}; \qquad m_k = -d_k - u_k \qquad (16c)$$

The underlined terms in Eq. (15) correspond to $\mathbf{P}_D(\mathbf{y}_n^{\nu+1}, k)$. Therefore, one gets

$$\mathbf{A}_k \Delta\mathbf{y}^{\nu+1}_{k,n} + d_k \cdot \mathbf{I}\, \Delta\mathbf{y}^{\nu+1}_{k-1,n} +$$

$$+ u_k \cdot \mathbf{I}\, \Delta\mathbf{y}^{\nu+1}_{k+1,n} \stackrel{!}{=} \mathbf{P}_D(\mathbf{y}^{\nu}_n, k) \qquad (17)$$

The LHS of this equation can be regarded as the product of the $(K \times J)^2$-matrix $\mathbf{P}'_D(\mathbf{y}^{\nu}_n)$ shown in Figure 2 and the vector $\Delta\mathbf{y}^{\nu+1}_n$. To obtain the correction one has to invert $\mathbf{P}'_D(\mathbf{y}^{\nu}_n)$:

$$\Delta\mathbf{y}^{\nu+1}_n = -\left[\mathbf{P}'_D(\mathbf{y}^{\nu}_n)\right]^{-1} \mathbf{P}_D(\mathbf{y}^{\nu}_n) \qquad (18)$$

Fortunately, due to its shape the matrix $\mathbf{P}'_D(\mathbf{y}^{\nu}_n)$ can be inverted very efficiently (Moussiopoulos, 1987): With

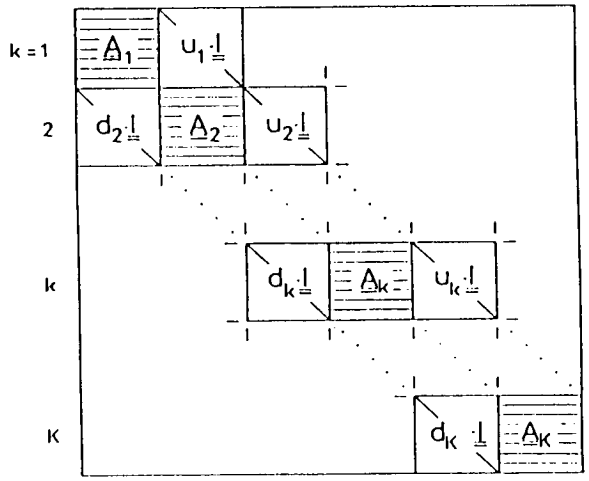

Figure 2 Sketch of the coefficient matrix $\mathbf{P}'_D(y_n^v)$.

the abbreviations $\mathbf{\Phi}_k \equiv \Delta y_{k,n}^{v+1}$ and $\mathbf{b}_k \equiv \mathbf{P}_D(y_n^v, k)$ one gets form Eq. (17) the equation system

$$\mathbf{A}_k \mathbf{\Phi}_k + d_k \mathbf{\Phi}_{k-1} + u_k \mathbf{\Phi}_{k+1} = \mathbf{b}_k; \quad k = 1, 2, \ldots, K \tag{19}$$

After introduction of the boundary condition at the model bottom (k = 0), Eq. (19) takes for k = 1 the form

$$\mathbf{A}_1^* 0_1 + u_1 0_2 = \mathbf{b}_1^* \tag{20}$$

Subsequently, an elimination step is performed by rewriting Eq. (19) as

$$\mathbf{A}_k^* \mathbf{\Phi}_k + u_k \mathbf{\Phi}_{k+1} = \mathbf{b}_k^*; \quad k = 2, 3, \ldots, K-1 \tag{21}$$

Taking into account the boundary condition at the model top one can solve for $\mathbf{\Phi}_K$ at once by inverting the J^2-matrix $\mathbf{A}_K^*$:

$$\mathbf{\Phi}_K = (\mathbf{A}_K^*)^{-1} \mathbf{b}_K^* \tag{22}$$

The remaining unknowns are computed by successive substitution into Eq. (21):

$$\mathbf{\Phi}_k = \left(\mathbf{A}_k^*\right)^{-1} (\mathbf{b}_K^* - u_k \mathbf{\Phi}_{k+1}); \quad k = K-1, K-2, \ldots, 1 \tag{23}$$

Obviously, the presented technique for inverting the matrix $\mathbf{P}'_D(y_n^v)$ resembles the well-known standard procedure for solving tridiagonal equation systems. The efficiency of this technique is due to the fact that the inversion of a $(K \times J)^2$-matrix can be replaced by 2K–1 inversions of J^2-matrices. This allows a substantial reduction of the computational expense compared with conventional inversion techniques.

During the iteration process both the order and the increment for the following time step are determined with the aid of the local error at solution level, i.e. from information provided by the algorithm itself. The Newton iteration is continued either until the residual is small compared to the estimated discretization error or until the correction is small compared to a prescribed tolerance. As an appropriate measure for the model accuracy, the global error can be optionally calculated in the course of the numerical solution.

3 Definition of the Reference Case

In order to estimate the feasible error caused by splitting the operators associated with diffusion and chemistry, the presented models were applied to simulate the ozone formation due to motor vehicle emissions in an urban area. To keep the comparative simulations clear and comprehensive we neglected deposition mechanisms and used for a particular discussion the compact chemical reaction mechanism of Eschenroeder and Martinez (1972), which has proved capable to provide a fairly good impression of photochemical reactions occuring in an urban airshed (Zellner and Moussiopoulos, 1986).

To demonstrate that the obtained results are not only valid in connection with the mechanism of Eschenroder and Martinez, comparative model simulations were also performed with the more detailed condensed ERT mechanism (Lloyd and Lurmann, 1985). The latter mechanism resulted from the well-known mechanism of Atkinson, Lloyd and Winges (1982) and takes into account 25 organic species, 10 of which are emitted.

The computational domain extended from surface of the constant height of 1000 m. As the vertical grid spacing influences the „computational" time scale of turbulent diffusion, simulations were performed using three different equidistant grids (Δz = 10, 20 and 50 m). Results obtained with both models showed only a minor influence of the grid spacing on the calculated concentration profiles. Therefore, in Section 4 only results obtained with the medium grid size (20 m) are presented and discussed in detail.

In the numerical simulations, photolysis rates were assumed to vary with solar radiation and to be height-independent. They were calculated from the position of the sun, sunrise being assumed at 6 a.m. and sunset at 8 p.m.. The eddy diffusivity K_{zz} was either assigned a constant value (10 m^2/s) or prescribed by an analytical expression allowing for an appropriate spatial and temporal variation (Figure 3; Dunst, 1980). For the emission rates of NO_x (assumed percentage of NO: 90 %) and hydrocarbons (80 % of which were classified as reactive) alternatively suitable diurnal variations and constant values were specified. The former followed from appropriate emission factors, a typical variation

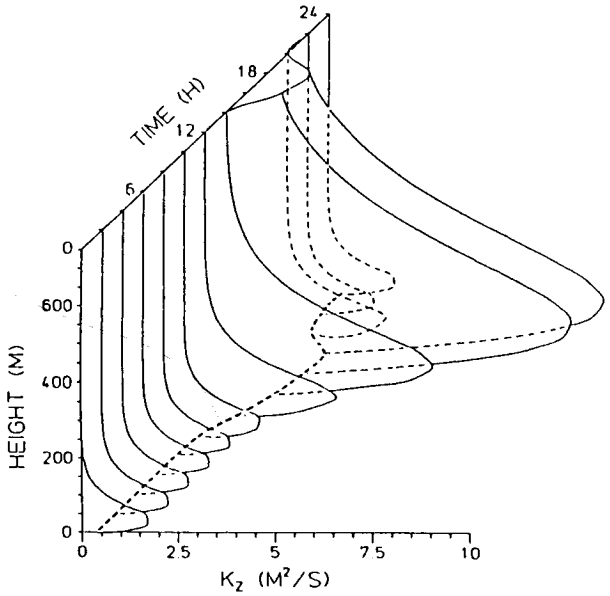

Figure 3 Assumed diurnal variation of vertical eddy diffusivity profiles.

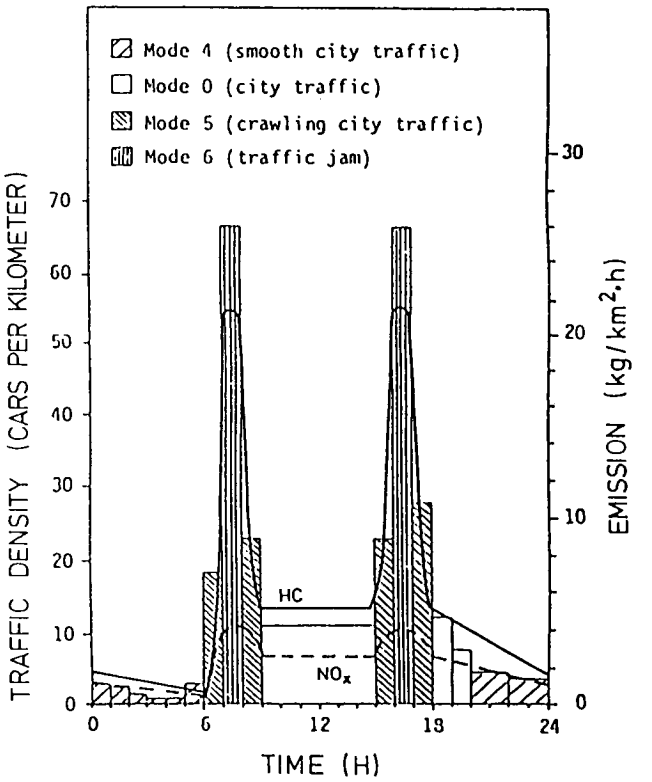

Figure 4 Typical diurnal variation of the traffic density, corresponding driving modes for an urban traffic lane and resulting diurnal variation of the nitrogen oxide and the hydrocarbon emission rates.

of the traffic density and corresponding driving modes (Figure 4; Moussiopoulos and Zellner, 1989), the latter represent daily mean values of the variable emissions. Correspondingly, four different model simulations were performed using the reaction mechanism of Eschenroeder and Martinez:

- Case KK, constant eddy diffusivity, constant emissions
- Case KV, constant eddy diffusivity, variable emissions
- Case VK, variable eddy diffusivity, constant emissions
- Case VV, variable eddy diffusivity, variable emissions

All these simulations were performed for an one-day period with the exception of case VV, where a three-day period was considered. Comparative simulations with the condensed ERT mechanism were performed only for case VV.

It is worthy of notice that prior to the actual comparative simulations excessive preliminary test calculations were performed, in the course of which the two models were proved to describe both vertical diffusive transport and chemical transformation *separately* in an almost identical manner. Therefore, any difference in the results of the comparative simulations can be doubtlessly attributed to the fact that the operators associated with diffusion and chemistry are splitted in only one of the two models.

4 Results for the Reaction Mechanism of Eschenroeder and Martinez

Figures 5 and 6 show the results of both models for the concentrations of NO, NO_2, ozone and reactive hydrocarbons (henceforth: RHC) at a height of 10 m above ground level for cases KK (a), KV (b), VK (c) and VV (d; first day). The results in Figure 5 were obtained with the Munich model, those in Figure 6 with the Karlsruhe model. In Figure 7 and 8 corresponding results are illustrated for case VV over a period of three days (7: Munich model, 8: Karlsruhe model), Figure 9 shows vertical concentration profiles computed with the Karlsruhe model for case VV and the same time period.

4.1 Intercomparison of Cases KK, KV, VK and VV

The results in Figures 5 and 6 reveal the decisive influence of the diurnal variation of the eddy diffusivity on the obtained concentrations: For the (spatially and temporally) constant value of 10 m^2/s only moderate concentration levels result and the diffusive transport dominates compared to chemical transformations, the latter resulting in an increase of the NO_2:NO ratio until sunset. The assumption of a constant value for the eddy

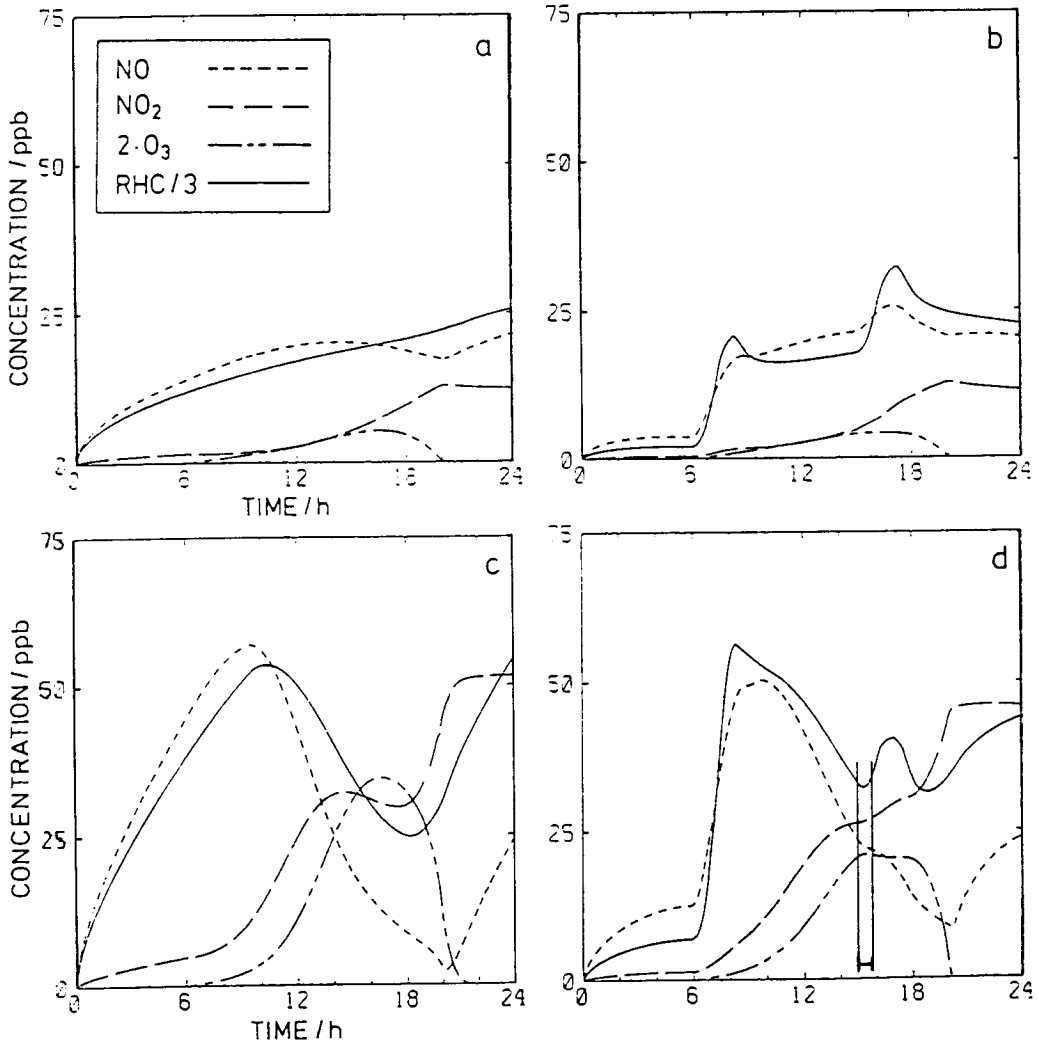

Figure 5 Time series (one day period) of the NO, NO_2, O_3 and RHC concentrations at a heigt of 10 m above ground level calculated with the Munich model for cases KK (a), KV (b), VK (c) and VV (d). The increment marked in (d) corresponds to the time period for which the analytic considerations in Section 4.3 are valid.

diffusivity is the reason that the actual diurnal variation of the emission rates only slightly affects the pollutant concentrations: Essentially, peaks of the NO and the RHC concentration appear which are associated with the elevated emissions during peak hour traffic (Figure 4).

If a more realistic diurnal variation for the eddy diffusivity is assumed (Figure 3), the pollutant concentrations vary considerably in the course of the day: In the case of constant emissions rather high amounts of NO and RHC accumulate close to the surface before sunrise as a consequence of the weak turbulent mixing. During the day, first NO_2 is rapidly formed reaching its peak value in the early afternoon. In spite of the intense turbulent mixing, NO_2 does not decrease considerably in the late afternoon, due to photochemical production. On the contrary, RHC and especially NO drastically decrease. As a result of the rapid increase of the NO_2:NO ratio, ozone is formed, reaching its maximum value around 16.30 h. The assumption of variable emissions in conjunction with the variable turbulent diffusion affects the diurnal concentration variation: Lower pollutant concentrations at sunrise lead to a slower and less intense photosmog formation. Higher NO emissions during the day result in a lower NO_2:NO ratio and hence also in weaker ozone formation.

The numerical simulations for case VV over the period of three days reveal that after the rapid decrease of turbulent mixing in the evening, ozone can persist in the region of low turbulence above the height of the nocturnal surface layer (Figure 9). Due to the absence of any pollutant removal mechanisms in the second and third days the oxidant formation intensity exceeds that of the first day and hence NO remains at very low levels (Figures 7–9). Contrary to the ozone maximum concentration which remains essentially unchanged between

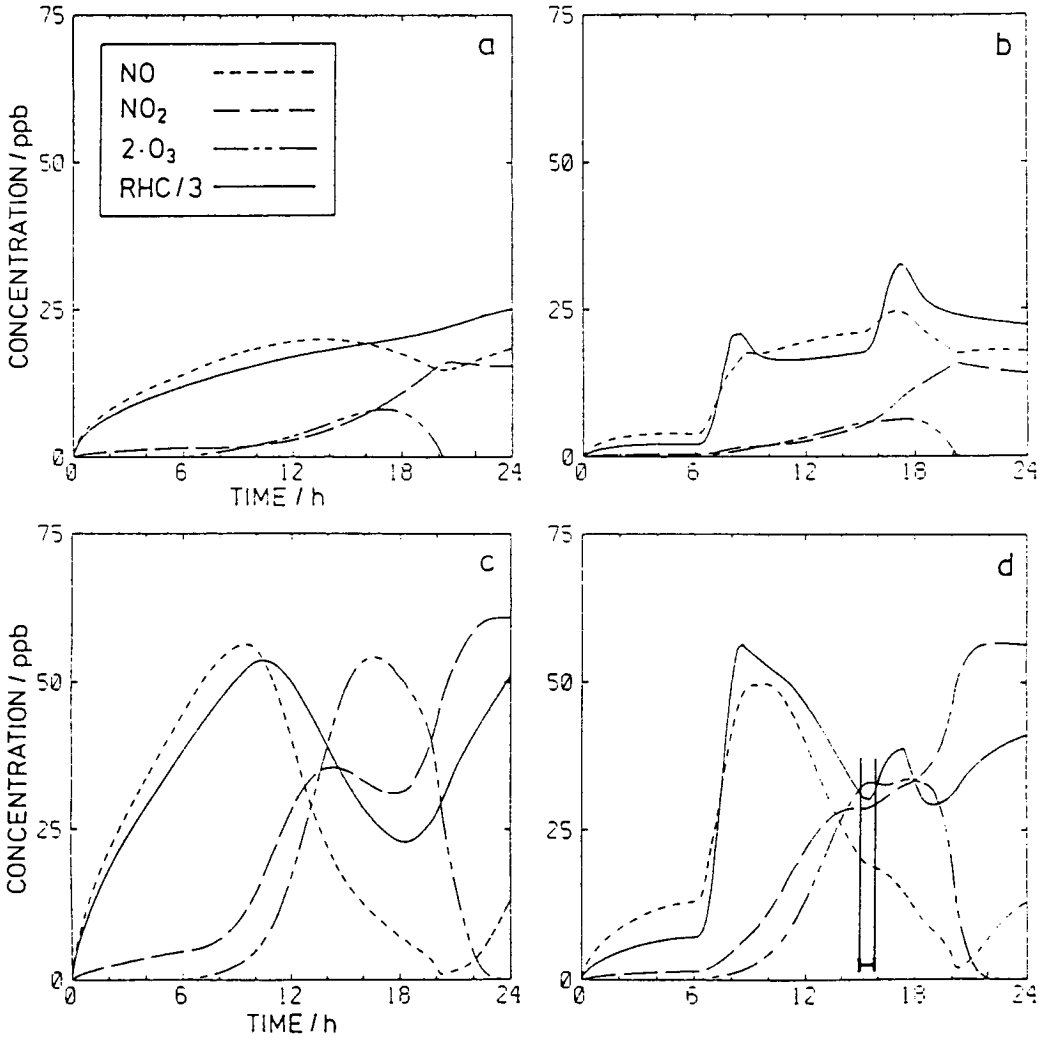

Figure 6 Same as Figure 5 but calculated with the Karlsruhe model.

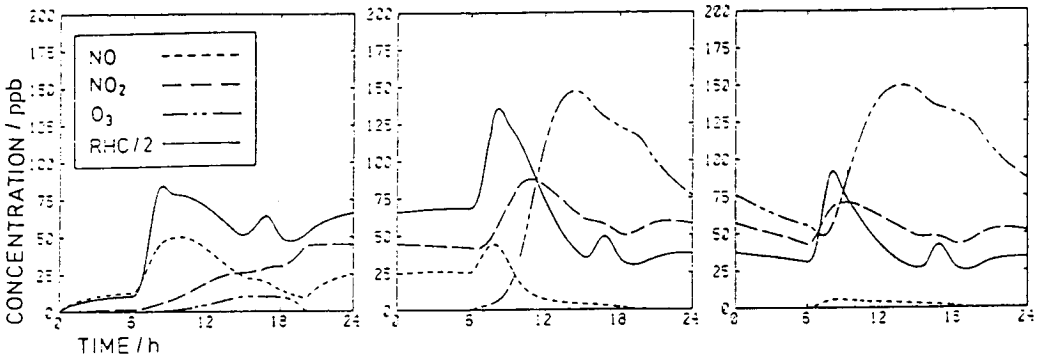

Figure 7 Time series (three day period) of the NO, NO_2, O_3 and RHC concentrations at a height of 10 m above ground level calculated with the Munich model for case VV.

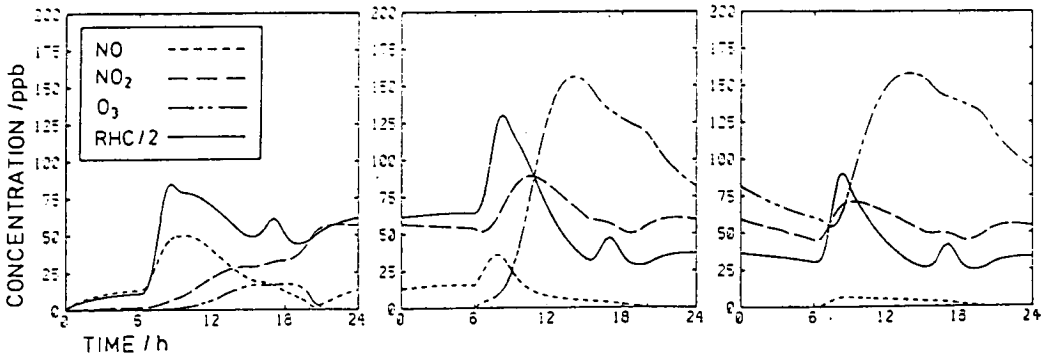

Figure 8 Same as Figure 7 but calculated with the Karlsruhe model.

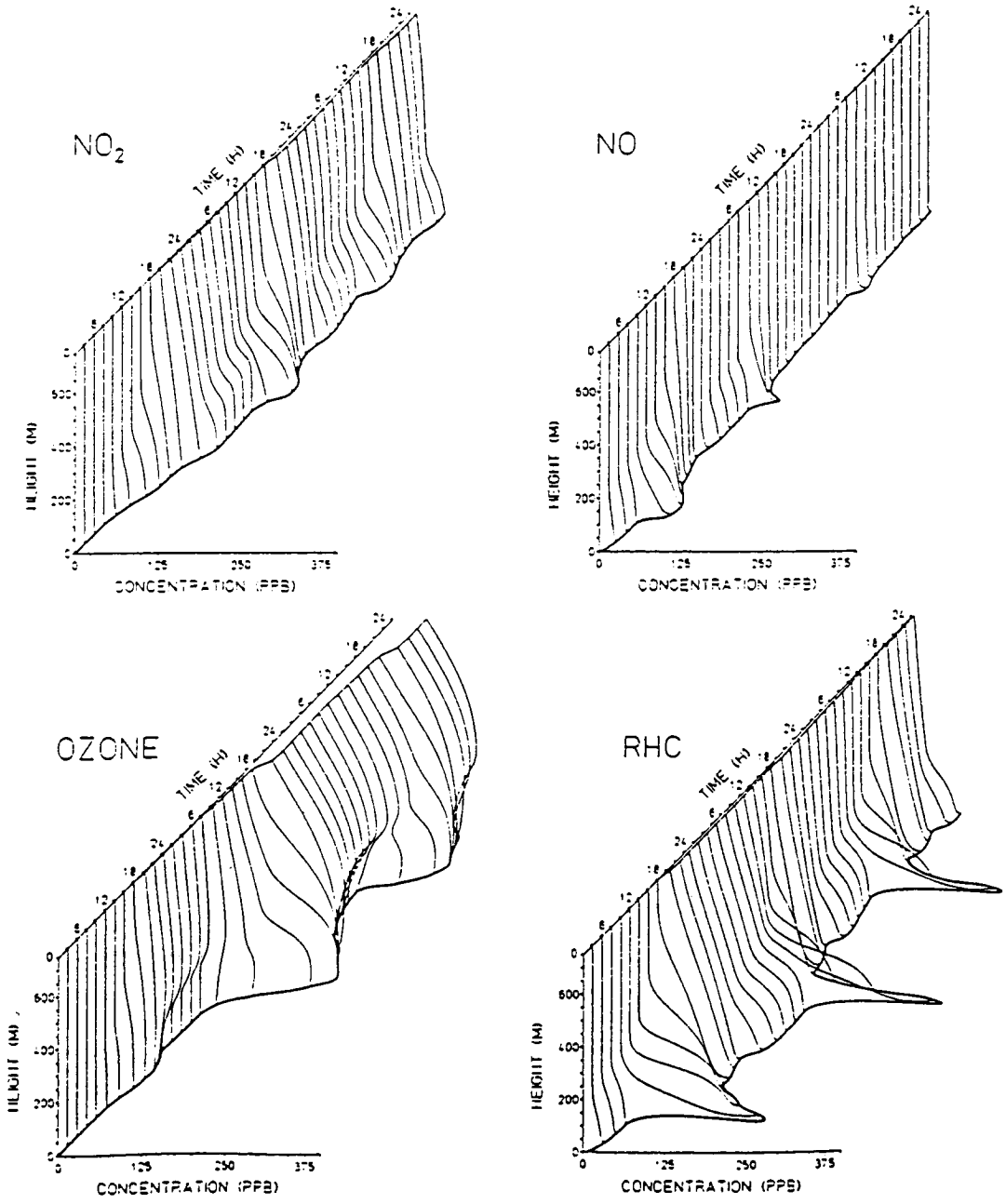

Figure 9 Diurnal variation of the vertical concentration profiles of NO, NO_2, O_3 and RHC calculated with the Karlsruhe model for case VV.

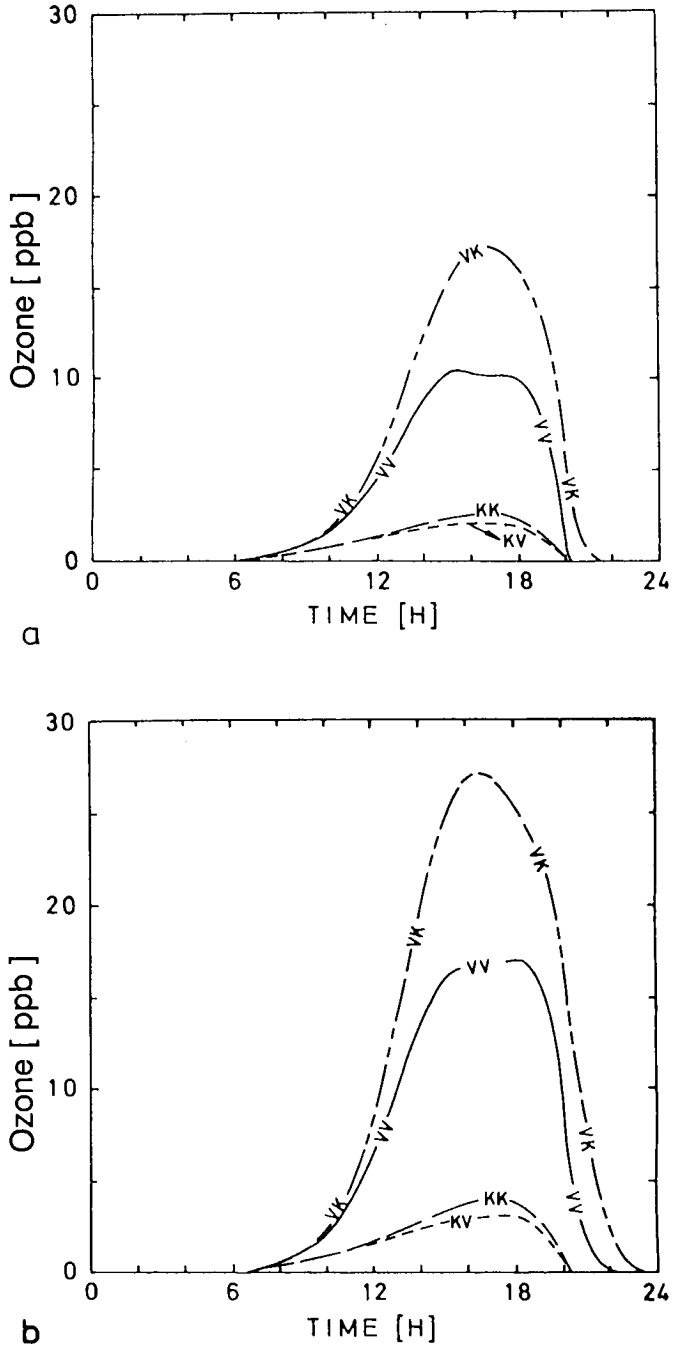

Figure 10 Time series (one day period) of the O_3 concentration at a height of 10 m above ground level for all considered cases. (a) Results of the Munich model. (b) Results of the Karlsruhe model.

the second and the third day, the daily mean ozone concentration in the third day is considerably higher than in the second day. This is associated with an extremely high NO_2:NO ratio revealing the magnitude of the photosmog potential in the third day. This magnitude exceeds by far the actual intensity of the photochemical reaction system. The situation in polluted areas resembles rather that of the first day of the simulation (Güsten, 1986).

4.2 Intercomparison of the Results of the Two Models

A comparison of Figures 5 and 7 with Figures 6 and 8 shows that in a qualitative sense both models lead to comparable results. Quantitatively, however, noticeable differences result, especially in the first day of the simulation. As stated above, the photosmog potential in the first day of the simulation resembles the situation frequently observed in polluted areas. Therefore, in the following the deviations of the results of the two models for the first day will be discussed in more detail.

Figure 10 shows the ozone concentration at a height of 10 m calculated by both models for the first day of the simulation and all cases KK, KV, VK and VV. In all these cases the Munich model systematically leads to lower ozone concentrations compared with the Karlsruhe model. Additional information can be extracted from the vertical profiles of the NO and the ozone concentration shown in Figure 11. These profiles were calculated with the two models for case VV at four times of the first day of the simulation. The deviations of the model results referring to the NO concentration profiles are much smaller than those referring to the vertical distribution of the ozone concentration. The Munich model predicts higher NO concentration which is apparently consistent with the obtained lower ozone levels. It is interesting that the deviation of the model results for the vertical profile of the ozone concentration drastically increase in the course of the day: The maximum ozone concentration calculated with the Karlsruhe model for 20.00 h exceeds the one obtained with the Munich model by more than 100 %. It should be noted, however, that the maximum values occur at almost the same height.

The concentration isopleths illustrated in Figure 12 reveal the time and height dependence of the Munich and Karlsruhe model results for case VV in the first day of the simulation. This figure confirms the fairly good qualitative agreement of the model results but at the same time proves that major deviations occur in the later afternoon and in the evening.

As stated at the end of Section 3, appropriate preliminary tests with the two models allow to conclude that deviations of the model results are solely attributed to the fact that in the Munich model vertical diffusive transport is decoupled from chemical kinetics, while in the Karlsruhe model no operator splitting is performed. In the following, we discuss further the detected deviations by the aid of a simplified analytic approach.

4.3 Simplified Analytic Considerations

In order to estimate how a decoupling of the operators associated with vertical diffusive transport and chemi-

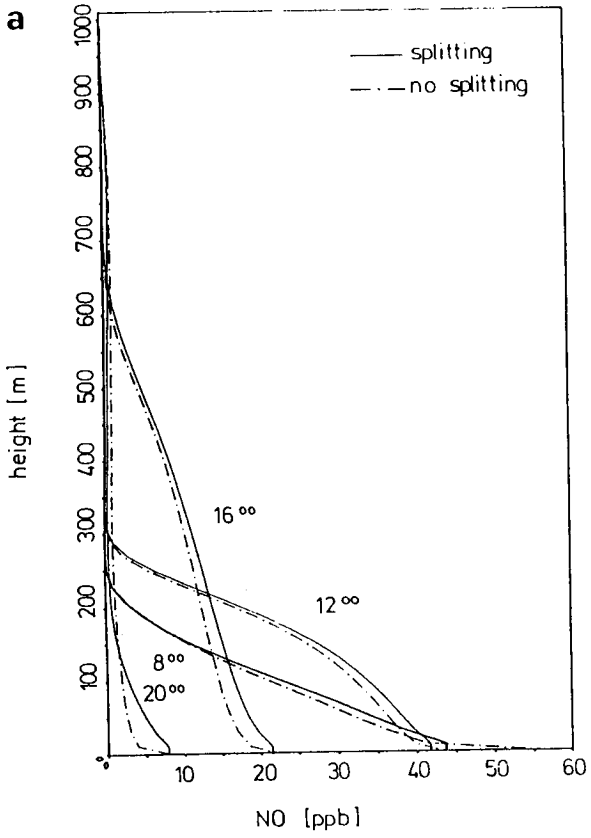

Figure 11 Vertical concentration profiles NO (a) and O_3 (b) calculated for the case VV at four different times (—— Munich model; — . — Karlsruhe model).

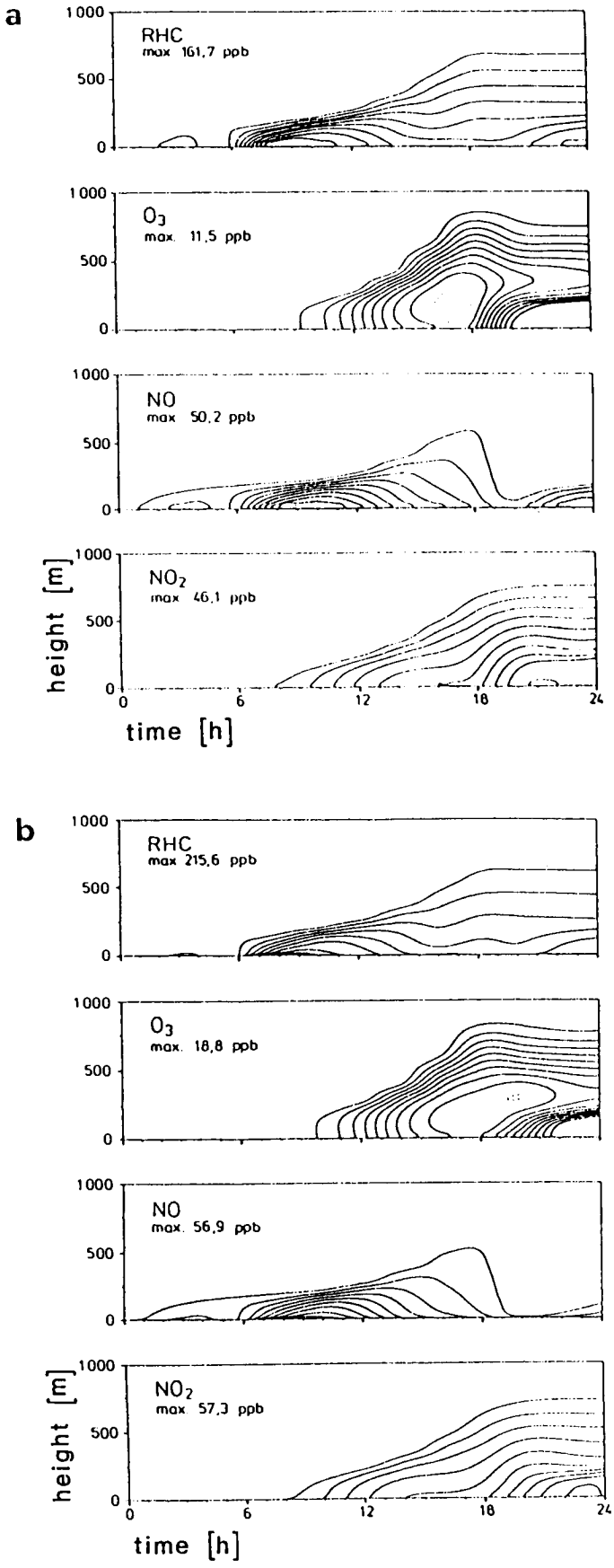

Figure 12 Time height cross sections of the RHC, O_3, NO and NO_2 concentrations for the case VV. (a) Results of the Munich model. (b) Results of the Karlsruhe model.

cal kinetics may affect the calculated pollutant concentrations, we consider the situation close to the ground during a limited time period in the late afternoon of the first day of the simulation. This time period is marked in Figures 5d and 6d. Let the approximation

$$\frac{dc_{NO}}{dt} = A - B\, c_{NO} \tag{24}$$

be valid for the change in the NO concentration during the considered time period. According to the mechanism of Eschenroeder and Martinez, at times of a rather low photosmog potential the chemical depletion rate of NO is approximately proportional to c_{O_3}. As the ozone concentration does not vary considerably in the time period of interest (Figures 5d and 6d), B in Eq. (24) is approximately constant. In the late afternoon the transport of NO originating from ground level emissions largely exceeds the chemical production of NO. If the corresponding supply rate of NO A is regarded as constant as well, the solution of Eq. (24) with $c_{NO}(t_0) = c_0$ reads

$$c_{NO} = c_o\, e^{-B(t-t_0)} + \frac{A}{B}(1 - e^{-B(t-t_0)}) \tag{25}$$

In contrast to this solution representing a coupled treatment of turbulent transport and chemistry, operator splitting would require solving sequentially the equations

$$\frac{dc_{NO}}{dt} = -b\, c_{NO}; \qquad \frac{dc_{NO}}{dt} = A \tag{26}$$

for successive integration steps with the time increment Δt. The first two steps can be written as

$$\tilde{c}_{NO,o} = c_o\, e^{-B\,\Delta t} \qquad c_{NO,1} = \tilde{c}_{NO,o} + A\,\Delta t \tag{27a}$$

$$\tilde{c}_{NO,1} = c_{NO,1}\, e^{-B\,\Delta t} \qquad c_{NO,2} = \tilde{c}_{NO,1} + A\,\Delta t \tag{27b}$$

After a total of i steps one gets finally

$$c_{NO,i} = c_o\, e^{-B\,i\,\Delta t} + A\,\Delta t \frac{1 - e^{-B\,i\,\Delta t}}{1 - e^{-B\,\Delta t}} \tag{28}$$

or, with $c_{NO} = c_{NO,i}$ and $i\,\Delta t \equiv t - t_o$

$$c_{NO} = c_o\, e^{-B(t-t_0)} + \frac{A}{B}\frac{B\,\Delta t}{1 - e^{-B\,\Delta t}}(1 - e^{-B(t-t_0)}) \tag{29}$$

A comparison of Eqs. (25) and (29) shows that because of

$$\frac{B\,\Delta t}{1 - 1 + B\,\Delta t - \frac{1}{2}(B\,\Delta t)^2 + \ldots} \approx \frac{1}{1 - \frac{1}{2}B\,\Delta t} \geq 1 \tag{30}$$

operator splitting should lead to an overestimation of the NO concentration. This corresponds to the detected deviation of the model results (Section 4.2).

If the considerations leading to Eq. (30) hold, a reduction of the time increment Δt should result in a smaller deviation of the model results. To verify this assumption, additional simulations of case VV were performed with the Munich model for several time increments Δt. Figure 13 shows vertical profiles of the ozone concentration at 20.00 h of the first day and several values of Δt. Although the results of the Munich model differ significantly from those of the Karlsruhe model even for the shortest considered time increment (Δt = 10 s), a reduction of Δt from 80 s to 10 s leads to the expected decrease of the model result deviation.

In the following it is shown that an overestimation of the NO concentration may lead to an even higher underestimation of the ozone concentration. As a starting point, Eq. (24) is assumed to be valid in the considered time period (Figures 5d and 6d) for ozone as

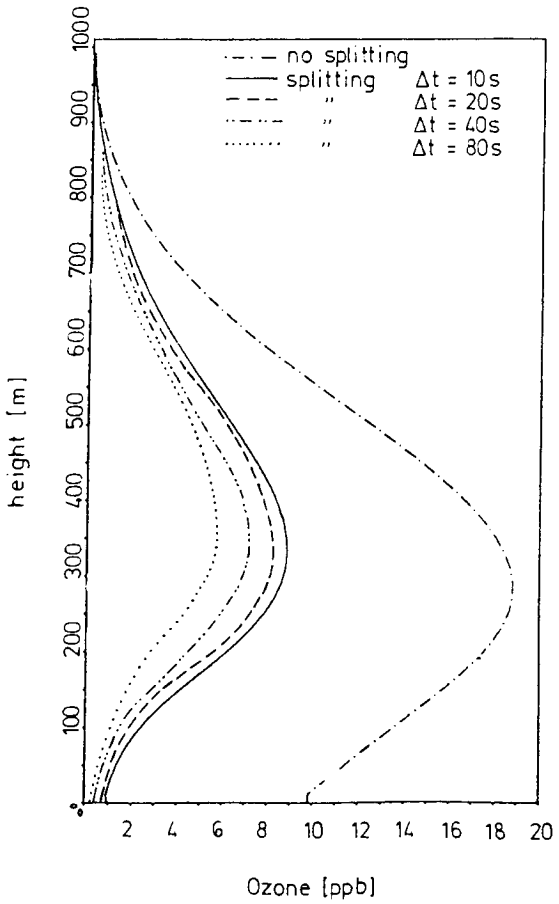

Figure 13 Vertical profiles of the O_3 concentration at 20.00 h of the first day calculated for the case VV with the Munich model using different time increments Δt. The result of the Karlsruhe model (— . —) is repeated for comparison.

well (production rate: A'; depletion rate: $B' c_{O3}$). The chemical production of ozone is associated with the photolysis of NO_2 and hence reads $k_{1*} c_{NO_2}$ [$k_{1*,max} \approx 0.5\ min^{-1}$; Moussiopoulos und Zellner, 1989]. Compared to the chemical production, in the time period of interest the vertical transport of ozone has a rather small influence on the surface level ozone concentration. Therefore, it is justified to assume

$$A' = k_{1*} c_{NO_2} \tag{31}$$

While in the late afternoon k_{1*} decreases and c_{NO_2} increases with time, as a crude approximation A' can be regarded as constant. According to the reaction mechanism of Eschenroeder and Martinez (1972) the depletion rate of ozone reads

$$B' c_{O_3} = (k_3 c_{NO} + k_{10} c_{RHC})\, c_{O_3} \tag{32}$$

If the changes in the concentrations of NO and RHC during the considered time period are neglected, B' can be regarded as constant. Its magnitude is of the order of $0.01\ s^{-1}$. With these assumptions the ozone concentration would be given by an equation similar to Eq. (25) which would converge within a few minutes to

$$c_{O_3} = \frac{A'}{B'} = \frac{k_{1*} c_{NO_2}}{k_3 c_{NO} + k_{10} c_{RHC}} \tag{33}$$

With the additional assumption $c_{NO} + c_{NO_2} = c_{NO_x} \approx$ const, which in view of Figures 5d and 6d appears to be justified as well, one gets, after differencing with respect to c_{NO} and rearranging

$$\frac{dc_{O_3}}{c_{O_3}} = -\frac{k_3 c_{NO_x} + k_{10} c_{RHC}}{k_3 c_{NO} + k_{10} c_{RHC}} \frac{c_{NO}}{c_{NO_2}} \frac{dc_{NO}}{c_{NO}} \tag{34}$$

The mechanism of Eschenroeder and Martinez yields $k_3/k_{10} \approx 3200$. As c_{NO}, c_{NO_2} and c_{RHC} are of the same order of magnitude, Eq. (34) can be simplified to read

$$\frac{dc_{O_3}}{c_{O_3}} \approx -\left(1 + \frac{c_{NO}}{c_{NO_2}}\right) \frac{dc_{NO}}{c_{NO}} \tag{35}$$

Obviously, an overestimation of the NO concentration will lead to an underestimation of the ozone concentration, the magnitude of which is governed by the ratio c_{NO}/c_{NO_2}. As this ratio is relatively high in the first day of the simulation, a small overestimation of the NO concentration associated with operator splitting causes in the course of that day a considerable underestimation of the ozone concentration. It is worthy of notice that the assumption c_{NO_x} a const leading to Eq. (34) is not valid during the second and the third days of the simulation as the concentrations of the hydroxy radical and the peroxy radical are high enough to facilitate the reactions of NO_2 to HNO_3 and PAN.

5 Results for the Condensed ERT Mechanism

The above discussion is not valid only in connection with the rather simple mechanism of Eschenroeder and Martinez, but may well be expected to hold also in case of more detailed chemical reaction mechanisms. To prove this, comparative simulations were also performed with the condensed ERT mechanism for the case VV (variable eddy diffusivity, variable emissions). As stated in Section 3, the grid spacing has no significant influence on the results of both models, so these simulations were carried out with the medium grid size of 20 m.

Figures 14a and 14b show the results of both models for the diurnal variation of the NO, NO_2 and ozone concentrations at a height of 10 m above ground level. Similar to the results discussed in the previous section, the ozone concentration is underpredicted by the Munich model. Hence, use of the operator splitting technique leads for both chemical reaction mechanisms used in the present paper to approximately 50 % lower ozone concentrations near the surface.

Contrary to the case of the mechanism of Eschenroeder and Martinez, in the case of the condensed ERT mechanism the Munich model leads to higher NO_2 concentrations near the surface compared to the Karlsruhe model. This might be attributed to differences in the description of the NO_2 oxidation to NO_3 due to the reaction

$$NO_2 + O_3 \rightarrow NO_3 \rightarrow O_2$$

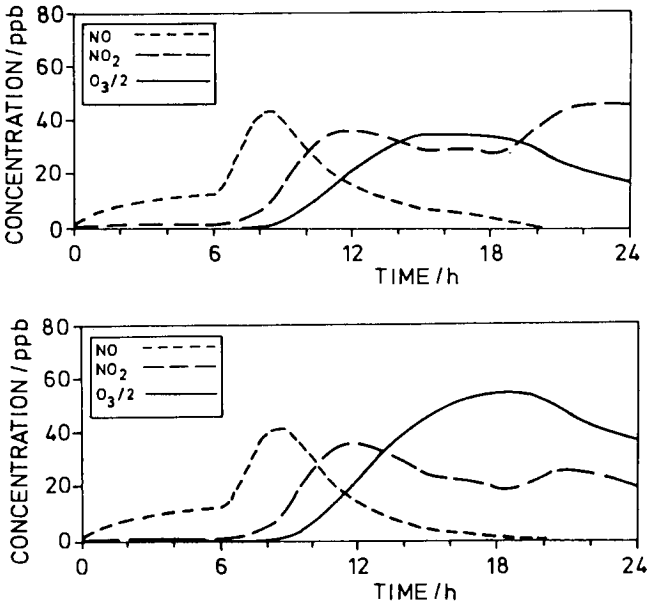

Figure 14 Time series (one day period) of the NO, NO_2 and O_3 concentrations at a height of 10 m above ground level calculated with (a) the Munich model and with (b) the Karlsruhe model.

This reaction has a chemical time scale of about 60 s. For the problem considered here, the characteristic time scale for vertical diffusion amounts to a few hundred seconds, i.e. is of the same order as the chemical time scale. Consequently, the deviations of the model results for the NO_2 concentration near the surface are most probably due to the operator splitting used in the Munich model.

In summary, intercomparison of model results using a detailed chemical reaction mechanism reveals differences in the predicted concentrations, notably in the ozone concentration near the surface, which are of the same order as in the case of a compact reaction mechanism.

6 Conclusions

The presented simulation results show that a model where the operators associated with vertical diffusion and chemistry are splitted yields pollutant concentrations which are qualitatively similar to those obtained without operator splitting. In a quantitative sense, however, the comparative simulations reveal that operator splitting may result in an overestimation of the NO concentration and a significant underestimation of the ozone concentration, especially at a rather low photosmog potential (i.e. a moderate c_{NO}/c_{NO_2} ratio).

Densely populated areas in industrialized countries are characterized by high NO_x emissions primarily exhausted as NO. In most cases the prevailing atmospheric transport and deposition mechanisms limit the intensity of the photosmog potential and thus usually result in moderate to high c_{NO}/c_{NO_2} ratios. In view of our results, the ozone concentration in such areas may be underpredicted by models where the operators associated with vertical diffusion and chemistry are splitted.

The results of this paper are valid in conjunction with the compact reaction mechanism of Eschenroeder and Martinez and the more detailed condensed ERT mechanism. If any other reaction mechanism is to be used within an atmospheric dispersion model and high accuracy is aimed at, comparative simulations analogous to those discussed in this paper should be considered as a possibility to estimate the feasible error caused by splitting the operators associated with vertical diffusion and chemistry.

References

Atkinson, R., A.C. Lloyd and *L. Winges,* 1982: An updated chemical mechanism for hydrocarbon/NOx/SO_2 photooxidations suitable for inclusion in atmospheric simulation models. Atmos. Environ. **16**, 1341–1355.

Dunst, M., 1980: Ergebnisse von Modellrechnungen zur Ausbreitung von Stoffbeimengungen in der planetarischen Grenzschicht. Zeitschr. Meteorol. **30**, 47–59.

Eschenroeder, A.Q. and *J.R. Martinez,* 1972: Concepts and applications of photochemical smog models. Adv. Chem. **113**, 101–167.

Graf, J., 1990: Simulation der Bildung und Verteilung von Ozon in der atmosphärischen Grenzschicht, PhD Dissertation, Universität München, Forschungsbericht DLR-FB 90–25.

Güsten, H., 1986: Formation, transport and control of photochemical smog, in The Handbook of Environmental Chemistry, Vol. 4A (O. Hutzinger, ed.), Springer Berlin, 53–105.

Lamb, R.G., 1973: Note on the application of K-theory to diffusion problems involving nonlinear chemical reactions. Atmos. Environ. **7**, 257–263.

Lloyd, A.C. and *F.W. Lurmann,* 1985: Chemical transformations in air quality models, in Handbook of Applied Meteorology (D.D. Houghton, ed.), Wiley, New York, 767–777.

McRae, G.J., W.R. Goodin and *J.H. Seinfeld,* 1982: Numerical solution of the atmospheric diffusion equation for chemically reacting flows. J. Comput. Phys. **45**, 1–42.

Moussiopoulos, N., 1987: A new technique for the solution of dispersion equation systems for reacting pollutants. Boundary-Layer Meteorol. **41**, 251–264.

Moussiopoulos, N., 1989: Mathematische Modellierung mesoskaliger Ausbreitung in der Atmosphäre, Fortschr.-Ber. VDI, Reihe 15.

Moussiopoulos, N. and *K. Zellner,,* 1989: Ozone formation from motorcar emissions, in: Encyclopedia of Environmental Control Technology, Vol. 2, Ch. 12, 763–806.

Roache, P.J., 1976: Computational Fluid Dynamics, Hermosa, Albuquerque, 446 pp.

Zellner, K. and *N. Moussiopoulos,* 1986: Simulations of the ozone formation caused by traffic in urban areas. Atmos. Environ. **20**, 1589–1596.